INT. J. CONTROL, 2003, VOL. 76, NO. 17, 1685–1698

Taylor & Francis
Taylor & Francis Group

Limit cycle analysis of the verge and foliot clock escapement using impulsive differential equations and Poincaré maps

ALEXANDER V. ROUP†, DENNIS S. BERNSTEIN†*, SERGEY G. NERSESOV‡, WASSIM M. HADDAD‡ and VIJAYSEKHAR CHELLABOINA§

The verge and foliot escapement mechanism of a mechanical clock is a classical example of a feedback regulator. In this paper we analyse the dynamics of this mechanism to understand its operation from a feedback perspective. Using impulsive differential equations and Poincaré maps to model the dynamics of this closed-loop system, we determine conditions under which the system possesses a limit cycle, and we analyse the period and amplitude of the oscillations in terms of the inertias of the colliding masses and their coefficient of restitution.

1. Introduction

Although clocks are one of the most important instruments in science and technology, it is not widely appreciated that feedback control has been essential to the development of accurate timekeeping. As described by Mayr (1970), feedback control played a role in the operation of ancient water clocks in the form of regulated valves. Alternative timekeeping devices, such as sundials, hourglasses and burning candles, were developed as well, although each of these had disadvantages.

Mechanical clocks were developed in the 12th century to keep both time and the calendar, including the prediction of astronomical events (Gimpel 1976, Landes 2000). Although early mechanical clocks were expensive, large and not especially accurate (they were often set using sundials), this technology for timekeeping had inherent advantages of accuracy and reliability as mechanical technology improved.

The crucial component of a mechanical clock is the *escapement*, which is a device for producing precisely regulated motion. The earliest escapement is the weight-driven *verge and foliot* escapement, which dates from the late 13th century. The feedback nature of the verge and foliot escapement is discussed in Lepschy *et al.* (1992) who point out that this mechanism is a work of 'pure genius'. Lepschy *et al.* (1992) have performed an important service in identifying this device as a contribution of automatic control technology.

It is interesting to note that the verge and foliot escapement was the only mechanical escapement known from the time of its inception until the middle of the 17th century. In 1657 Huygens modified the verge and foliot escapement by replacing the foliot with a pendulum swinging in a vertical plane and the crown gear mounted horizontally. However, the basic paddle/gear teeth interaction remained the same. The next escapement innovation was the invention of the anchor or recoil escapement by Hooke in 1651 in which a pendulum-driven lever arm alternately engages gear teeth in the same plane. Subsequent developments invoking additional refinements include the deadbeat escapement of Graham and the grasshopper escapement of Harrison. The latter device played a crucial role when the British Government sought novel technologies for determining longitude at sea (Sobel and Andrewes 1998). For details on these and other escapements, see Gazely (1956), Penman (1998), Headrick (2002) and Bernstein (2002). Since escapements produce oscillations from stored energy, they can be analysed as self-oscillating dynamical systems. For details, see Andronov *et al.* (1966).

The present paper considers only the verge and foliot escapement, which consists of a pair of rotating rigid bodies which interact through collisions. These collisions constitute feedback action which give rise to a limit cycle. This limit cycle provides the crown gear with a constant average angular velocity that determines the clock speed for accurate timekeeping.

The verge and foliot is analysed in Lepschy *et al.* (1992) under elastic and inelastic conditions. For the latter case expressions were obtained for the period of the limit cycle and for the crown gear angular velocity at certain points in time. Because of the presence of collisions, a hybrid continuous-discrete model was used to account for instantaneous changes in velocity.

The present paper extends the analysis of Lepschy *et al.* (1992) in several directions. In § 2 we provide a detailed model of the verge and foliot escapement for arbitrary values of the coefficient of restitution. In § 3 we show that impulsive differential equations are well-suited for modelling the dynamics of this system. The

Received 24 March 2003. Revised 25 September 2003.

* Author for correspondence. e-mail: dsbaero@umich.edu
†Department of Aerospace Engineering, The University of Michigan, Ann Arbor, MI 48109-2140, USA.
‡School of Aerospace Engineering, Georgia Institute of Technology, Atlanta, GA 30332-0150, USA.
§Mechanical and Aerospace Engineering, University of Missouri, Columbia, MO 65211-2200, USA.

International Journal of Control ISSN 0020–7179 print/ISSN 1366–5820 online © 2003 Taylor & Francis Ltd
http://www.tandf.co.uk/journals
DOI: 10.1080/0020717031000163241 2

mathematical properties of impulsive differential equations have been developed in Lakshmikantham *et al.* (1989) and Bainov and Simeonov (1989), and they have been used to model resetting absorbers in Bupp *et al.* (2000 a). Applications to mechanical systems with collisions are given in Brogliato (1999). Furthermore, Haddad *et al.* (2001 a) develop a general framework for non-linear impulsive dynamical systems by addressing stability, dissipativity, stability of feedback interconnections and optimality. Stability analysis of impulsive differential equations is also considered in Ye *et al.* (1998) and Chellaboina *et al.* (2003), with the latter presenting invariant set stability theorems for a class of non-linear impulsive dynamical systems. In § 4 we analyse the model obtained in § 3 to characterize the periodic orbit arising in the closed-loop dynamics. The main result is an expression for the average angular velocity of the crown gear in terms of the mechanical parameters and applied torque. In § 5 we give a brief review of recent results on Poincaré maps for impulsive differential equations developed in Grizzle *et al.* (2001) and Neresov *et al.* (2002). Then, in § 6 we use the results of § 5 to analyse the stability of periodic orbits arising in the escapement mechanism. In § 7 we provide a numerical illustration of the results presented in § 6. Finally, we draw conclusions in § 8.

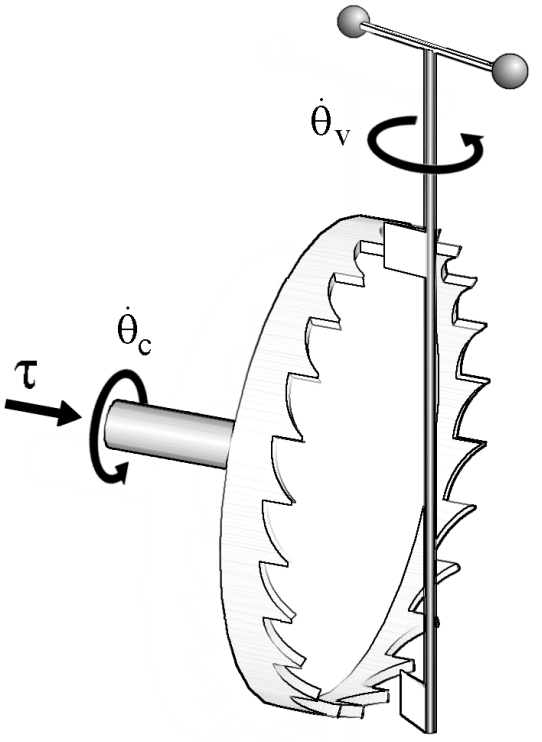

Figure 1. Verge and foliot escapement mechanism. The angular velocities of the crown gear and verge are $\dot{\theta}_c$ and $\dot{\theta}_v$, respectively, with the sign convention shown. There is a constant torque τ applied to the crown gear with positive direction shown.

2. Modelling

The verge and foliot escapement mechanism shown in figure 1 consists of two rigid bodies rotating on bearings. For simplicity we assume that these bearings are frictionless. The *crown gear* has teeth spaced equally around its perimeter. The *verge and foliot*, which henceforth will be referred to as the *verge*, has two paddles that engage the teeth of the crown gear through alternating collisions. We ignore sliding of the paddles along the crown gear teeth, which may occur in practice. For the orientation shown in figure 1, there is an upper paddle and a lower paddle.

Collisions involving the upper paddle impart a positive torque impulse to the verge, while those involving the lower paddle impart a negative torque impulse to the verge. Each collision imparts a negative torque impulse which acts to retard the motion of the crown gear. The mechanism is driven by a constant torque applied to the crown gear. This torque is usually provided by a mass hanging from a rope which is wound around the shaft. The verge spins freely at all times except at the instant a collision takes place. Energy is assumed to leave the system only through the collisions. The amount of energy lost during each collision is a function of the system geometry as well as the coefficient of restitution e realized in the collision.

The crown gear and verge have inertias I_c and I_v, contact radii r_c and r_v, and angular velocities $\dot{\theta}_c$ and $\dot{\theta}_v$, respectively. The velocities immediately before and after a collision are denoted by the subscripts 0 and 1, respectively, as in $\dot{\theta}_{c_0}$ and $\dot{\theta}_{c_1}$. The motion of the crown gear and verge is governed by the differential equations

$$\ddot{\theta}_c(t) = \frac{1}{I_c}\tau - \frac{r_c}{I_c}F(\theta_c(t), \theta_v(t), \dot{\theta}_c(t), \dot{\theta}_v(t)) \tag{1}$$

$$\ddot{\theta}_v(t) = \begin{cases} +(r_v/I_v)F(\theta_c(t), \theta_v(t), \dot{\theta}_c(t), \dot{\theta}_v(t)), & \text{upper} \\ -(r_v/I_v)F(\theta_c(t), \theta_v(t), \dot{\theta}_c(t), \dot{\theta}_v(t)), & \text{lower} \end{cases} \tag{2}$$

where the first expression in (2) applies to collisions between the crown gear and the upper paddle, and the second expression applies to collisions between the crown gear and the lower paddle. The function $F(\theta_c(t), \theta_v(t), \dot{\theta}_c(t), \dot{\theta}_v(t))$ is the collision force, which is zero when the crown gear and verge are not in contact and is impulsive at the instant of impact. The collision force function F acts equally and oppositely on the crown gear and verge. Defining

$$\sigma \triangleq \begin{cases} +1, & \text{upper} \\ -1, & \text{lower} \end{cases} \tag{3}$$

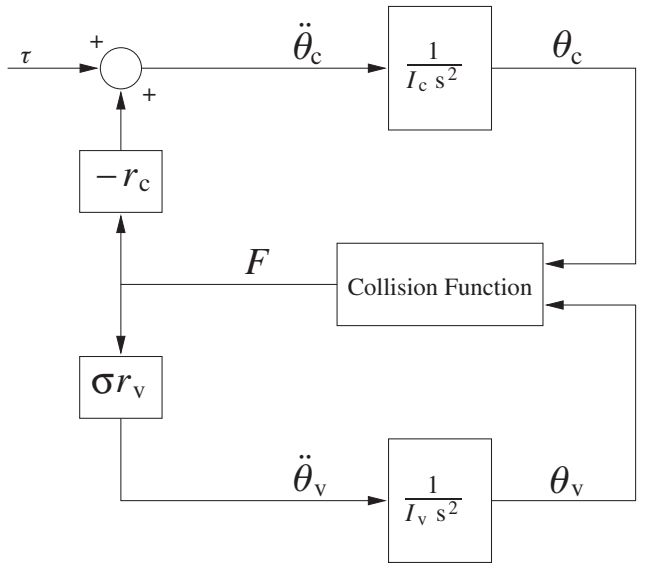

Figure 2. System block diagram showing the interconnection of the crown gear and verge rigid bodies through the collision block.

equation (2) can be written in the form

$$\ddot{\theta}_v(t) = \sigma \frac{r_v}{I_v} F(\theta_c(t), \theta_v(t), \dot{\theta}_c(t), \dot{\theta}_v(t)). \tag{4}$$

A system diagram is shown in figure 2.

To determine the collision force function, we integrate (1) and (4) across a collision event to obtain

$$\dot{\theta}_{c_1} - \dot{\theta}_{c_0} = \lim_{\Delta t \to 0} \left(\frac{1}{I_c} \int_{t-\Delta t}^{t+\Delta t} \tau \, ds - \frac{r_c}{I_c} \int_{t-\Delta t}^{t+\Delta t} F(s) \, ds \right) \tag{5}$$

$$\dot{\theta}_{v_1} - \dot{\theta}_{v_0} = \lim_{\Delta t \to 0} \left(\sigma \frac{r_v}{I_v} \int_{t-\Delta t}^{t+\Delta t} F(s) \, ds \right) \tag{6}$$

Eliminating the integrated collision force from (5) and (6) yields

$$\frac{\sigma I_v}{r_v} \dot{\theta}_{v_0} + \frac{I_c}{r_c} \dot{\theta}_{c_0} = \frac{\sigma I_v}{r_v} \dot{\theta}_{v_1} + \frac{I_c}{r_c} \dot{\theta}_{c_1} \tag{7}$$

which is an expression of conservation of linear momentum at the instant of a collision. Expression (7) can be rewritten as

$$M_v V_{v_0} + M_c V_{c_0} = M_v V_{v_1} + M_c V_{c_1} \tag{8}$$

where $M_c \triangleq I_c / r_c^2$ and $M_v \triangleq I_v / r_v^2$ are the effective crown gear mass and effective verge mass, respectively, and $V_c \triangleq r_c \dot{\theta}_c$ and $V_v \triangleq \sigma r_v \dot{\theta}_v$ are the tangential velocities of the crown gear and the verge, respectively.

The coefficient of restitution e relates the linear velocities of the crown gear and the verge before and after the collision according to

$$V_{c1} - V_{v1} = -e(V_{c0} - V_{v0}) \tag{9}$$

which accounts for the loss of kinetic energy in a collision. Solving (7) and (9) yields

$$\Delta\dot{\theta}_c = -\frac{M_v(1+e)}{r_c(M_v + M_c)} V_{c0} + \sigma \frac{M_v(1+e)}{r_c(M_v + M_c)} V_{v0} \tag{10}$$

$$\Delta\dot{\theta}_v = \sigma \frac{M_c(1+e)}{r_v(M_v + M_c)} V_{c0} - \frac{M_c(1+e)}{r_v(M_v + M_c)} V_{v0} \tag{11}$$

where

$$\Delta\dot{\theta}_c \triangleq \dot{\theta}_{c_1} - \dot{\theta}_{c_0}, \qquad \Delta\dot{\theta}_v \triangleq \dot{\theta}_{v_1} - \dot{\theta}_{v_0} \tag{12}$$

are the impulsive changes in angular velocity when a collision occurs. These quantities depend on the geometry as well as the velocities immediately before the collision. The integral of the impulsive force function over a collision event is

$$\int_{t_0}^{t_1} F(s) \, ds = \frac{M_c M_v (1+e)}{M_v + M_c} (V_{c0} - V_{v0}) \tag{13}$$

where t_0 is a time slightly before the collision and t_1 is a time slightly after the collision.

3. Impulsive differential equations

In this section we rewrite the equations of motion of the escapement mechanism in the form of an impulsive differential equation. An impulsive differential equation is described by three components; namely, a *continuous-time differential equation*, which governs the system state between impulses, an *impulse equation*, which models an impulsive jump defined by a *jump function* at the instant an impulse occurs, and a *jump criterion*, which defines a set of jump events in which the impulse equation is active. These components can be written in the form

$$\dot{x}(t) = f_c(x(t)), \qquad x(t) \notin \mathcal{S} \tag{14}$$

$$\Delta x(t) = f_d(x(t)), \qquad x(t) \in \mathcal{S} \tag{15}$$

where $t \geq 0$, $x(t) \in \mathbb{R}^n$, $f_c : \mathbb{R}^n \to \mathbb{R}^n$ is locally Lipschitz continuous; $f_d : \mathbb{R}^n \to \mathbb{R}^n$ is continuous; and $\mathcal{S} \subset \mathbb{R}^n$ is the jump set. For the remainder of the paper we refer to (14) and (15) as the impulsive dynamical system $\mathcal{G}$.

To describe the dynamics of the verge and foliot escapement mechanism as an impulsive differential equation, define the state

$$x = [\, x_1 \quad x_2 \quad x_3 \quad x_4 \,]^T \triangleq [\, \theta_c \quad \theta_v \quad \dot{\theta}_c \quad \dot{\theta}_v \,]^T \tag{16}$$

where x_1 is the position of the crown gear, that is, the counterclockwise angle swept by the line connecting the centre of the crown gear and the zeroth tooth from the 12 o'clock position; x_2 is the position of the verge, that is, the deviation of the mean line of the angular offset between two paddles from the vertical plane perpendicular to the plane of the crown gear; x_3 is the angular

velocity of the crown gear; and x_4 is the angular velocity of the verge. Between collisions the state satisfies

$$\dot{x}(t) = \begin{bmatrix} 0 & 0 & 1 & 0 \\ 0 & 0 & 0 & 1 \\ 0 & 0 & 0 & 0 \\ 0 & 0 & 0 & 0 \end{bmatrix} x(t) + \begin{bmatrix} 0 \\ 0 \\ 1/I_c \\ 0 \end{bmatrix} \tau \qquad (17)$$

while the jump function is given by

$$f_d(x) = \begin{bmatrix} 0 & 0 & 0 & 0 \\ 0 & 0 & 0 & 0 \\ 0 & 0 & -r_c\, G_c & \sigma r_v\, G_c \\ 0 & 0 & \sigma r_c\, G_v & -r_v\, G_v \end{bmatrix} x \qquad (18)$$

where

$$G_c \triangleq \frac{(I_v/r_v^2)(1+e)}{r_c((I_v/r_v^2)+(I_c/r_c^2))}, \quad G_v \triangleq \frac{(I_c/r_c^2)(1+e)}{r_v((I_v/r_v^2)+(I_c/r_c^2))} \qquad (19)$$

The jump set is

$$\mathcal{S} = \left\{ \bigcup_{m=0}^{n} \mathcal{S}_m^{\text{upper}} \right\} \bigcup \left\{ \bigcup_{m=0}^{n} \mathcal{S}_m^{\text{lower}} \right\} \qquad (20)$$

where, for $m = 0, \ldots, n$

$$\begin{aligned} \mathcal{S}_m^{\text{upper}} = \{x:\, & r_c \sin(x_1 - m\,\alpha_c) = r_v \tan(x_2 + \alpha_v/2), \\ & r_c x_3 - r_v x_4 > 0, (m - 1/2)\alpha_c + 2p\pi \le x_1 \\ & \le (m + 1/2)\alpha_c + 2p\pi, p \in \{0, 1, 2, \ldots\}\} \end{aligned} \qquad (21)$$

$$\begin{aligned} \mathcal{S}_m^{\text{lower}} = \{x:\, & r_c \sin(m\alpha_c - x_1) = r_v \tan(-x_2 + \alpha_v/2), \\ & r_c x_3 + r_v x_4 > 0, (m - 1/2)\alpha_c + (2p-1)\pi \le x_1 \\ & \le (m + 1/2)\alpha_c + (2p-1)\pi, p \in \{0, 1, 2, \ldots\}\} \end{aligned} \qquad (22)$$

where α_c is the angle between neighbouring teeth on the crown gear, α_v is the angular offset of the paddles about the vertical axis, m is the index of the crown gear tooth involved in the collision and p is the number of full rotations of the crown gear. The crown gear teeth are numbered from 0 to n clockwise, or opposite the direction of increasing θ_c, beginning at $\theta_c = 0$. There must be an odd number of crown gear teeth for the mechanism to function correctly, and thus n is even.

4. Characterization of periodic orbits

In this section we characterize periodic orbits of $\mathcal{G}$. First we integrate the continuous-time dynamics (17) to obtain

$$\theta_{c_2} = \theta_{c_0} + \dot{\theta}_{c_1} \Delta t + \frac{\tau}{2I_c} \Delta t^2 \qquad (23)$$

$$\theta_{v_2} = \theta_{v_0} + \dot{\theta}_{v_1} \Delta t \qquad (24)$$

where θ_{c_2} and θ_{v_2} are evaluated immediately before the next collision and Δt is the elapsed time between two successive collisions. For an initial collision involving the upper paddle we have

$$r_c \sin(\theta_{c_0} - m\alpha_c) = r_v \tan(\theta_{v_0} + \alpha_v/2) \qquad (25)$$

The index m' of the crown gear tooth involved in the subsequent lower collision is given by

$$m' = m + \pi/\alpha_c + 1/2 \qquad (26)$$

so that the condition

$$r_c \sin(m\alpha_c + \pi + \alpha_c/2 - \theta_{c_2}) = r_v \tan(-\theta_{v_2} + \alpha_v/2) \qquad (27)$$

must be satisfied at the lower collision. Substituting (23) and (24) into (27) yields

$$\begin{aligned} r_c \sin\left(\theta_{c_0} + \dot{\theta}_{c_1}\Delta t + \frac{\tau}{2I_c}\Delta t^2 - (m + \tfrac{1}{2})\alpha_c\right) \\ = r_v \tan\left(-\theta_{v_0} - \dot{\theta}_{v_1}\Delta t + \frac{\alpha_v}{2}\right) \end{aligned} \qquad (28)$$

A small angle approximation of (25) and (28) implies

$$r_c(\theta_{c_0} - m\alpha_c) = r_v\left(\theta_{v_0} + \frac{\alpha_v}{2}\right) \qquad (29)$$

$$\begin{aligned} r_c\left(\theta_{c_0} + \dot{\theta}_{c_1}\Delta t + \frac{\tau}{2I_c}\Delta t^2 - (m + \tfrac{1}{2})\alpha_c\right) \\ = r_v(-\theta_{v_0} - \dot{\theta}_{v_1}\Delta t + \frac{\alpha_v}{2}) \end{aligned} \qquad (30)$$

Subtracting (29) from (30) yields

$$r_c\dot{\theta}_{c_1}\Delta t + \frac{r_c\tau}{2I_c}\Delta t^2 - \tfrac{1}{2}r_c\alpha_c = -r_v\dot{\theta}_{v_1}\Delta t - 2r_v\theta_{v_0} \qquad (31)$$

Analogous expressions hold for collisions involving the lower paddle. Solving for Δt yields

$$\Delta t = \frac{-d + \sqrt{d^2 + (r_c\,\alpha_c - 4\sigma r_v\theta_{v_0})r_c\tau/I_c}}{r_c\tau/I_c} \qquad (32)$$

where

$$d = \frac{[(2+e)M_c - eM_v]r_c\dot{\theta}_{c_0}}{M_v + M_c} + \sigma\frac{[(2+e)M_v - eM_c]r_v\dot{\theta}_{v_0}}{M_v + M_c} \qquad (33)$$

Furthermore, the kinetic energy ΔT lost in a collision is given by

$$\Delta T = \frac{M_v\, M_c}{2\,(M_v + M_c)}\,(e^2 - 1)\,(r_v\,\dot{\theta}_{v_0} - \sigma r_c\,\dot{\theta}_{c_0})^2 \qquad (34)$$

Next, we specify conditions that characterize a periodic orbit in the $(\dot{\theta}_c, \dot{\theta}_v)$ plane. The first condition

$$\dot{\theta}_{v_1} = -\dot{\theta}_{v_0} \qquad (35)$$

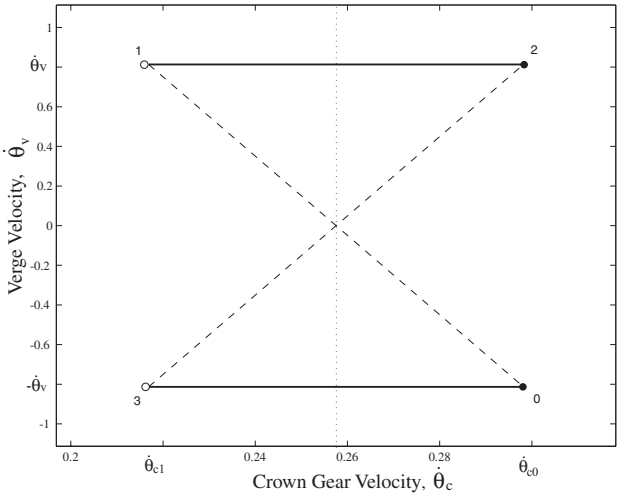

Figure 3. Velocity phase portrait of a representative periodic orbit. Instant 0 is prior to a collision with the upper paddle, 1 is after the collision, 2 is prior to the successive lower paddle collision, and 3 is after the second collision. The continuous-time trajectories are shown with solid lines and the impulsive jumps are shown with dashed lines. The average crown gear velocity is shown with a vertical dotted line.

requires the verge to reverse direction at every collision. This condition ensures that the absolute value of the verge speed is constant with time. On the other hand, the crown gear will lose speed with every collision and then gain speed between collisions. Thus, the second condition

$$\dot{\theta}_{c_1} = \dot{\theta}_{c_0} - \frac{\tau\,\Delta t}{I_c} \tag{36}$$

requires the crown gear speed to be the same before each collision. The third condition

$$\theta_{v_0} = -\theta_{v_2} \tag{37}$$

requires the range of motion of the verge between collisions to be centered at $\theta_{v_0} = 0$. This condition keeps the motion of the verge from wandering out of the range of angles within which the mechanism will work properly. A representative periodic orbit satisfying (35), (36) and (37) is shown in figure 3.

Next, we derive some properties of periodic orbits satisfying (35), (36) and (37). The average crown gear velocity $\overline{\dot{\theta}_c}$ of a periodic orbit is given by

$$\overline{\dot{\theta}_c} = \frac{\Delta T}{\tau\,\Delta t} \tag{38}$$

To obtain an expression for $\overline{\dot{\theta}_c}$ as a function of the applied torque and geometric parameters it follows from (7), (9) and (32)–(38) that

$$\overline{\dot{\theta}_c} = \frac{\sqrt{\tau}}{2r_c}\sqrt{\left(\frac{1-e}{1+e}\right)\frac{(M_c+M_v)\alpha_c}{M_c M_v}} \tag{39}$$

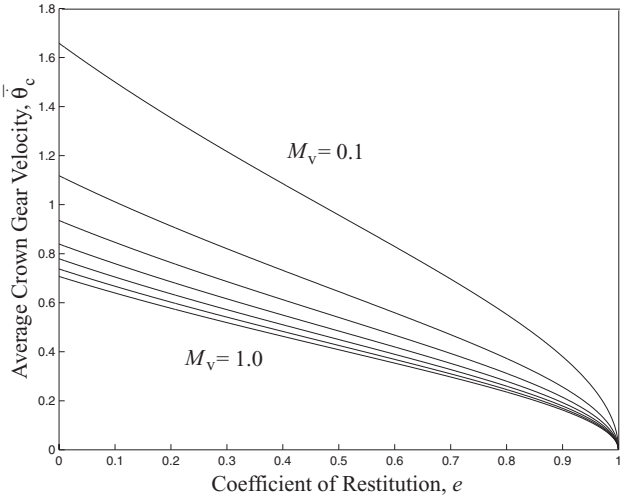

Figure 4. $\overline{\dot{\theta}_c}$ versus e for several values of M_v. The system parameters are $M_v = 0.10$, 0.25, 0.40, 0.55, 0.70, 0.85, and 1.00, increasing from the top curve to the bottom curve, $M_c = 1$, $r_c = 1$, $\tau = 1$, and $\alpha_c = 1$.

Figure 4 shows the sensitivity of $\overline{\dot{\theta}_c}$ to changes in the parameters e and M_v.

The crown gear velocity before a collision is given by

$$\dot{\theta}_{c_0} = \frac{(1-e)\,M_c + 2\,M_v}{(1-e)(M_c+M_v)}\,\overline{\dot{\theta}_c} \tag{40}$$

and the crown gear velocity after a collision is given by

$$\dot{\theta}_{c_1} = \frac{(1-e)\,M_c - 2\,e\,M_v}{(1-e)(M_c+M_v)}\,\overline{\dot{\theta}_c} \tag{41}$$

The verge velocity is given by

$$\dot{\theta}_v = \pm\frac{1}{2\,r_v}\sqrt{\left(\frac{1+e}{1-e}\right)\frac{M_c\,\alpha_c\,\tau}{(M_c+M_v)\,M_v}} \tag{42}$$

where the verge velocity is positive following a collision involving the upper paddle and negative following a collision involving the lower paddle. Finally, the period of this periodic orbit is

$$2\,\Delta t = \frac{\alpha_c}{\overline{\dot{\theta}_c}} \tag{43}$$

5. Stability analysis of periodic orbits using Poincaré maps

In the previous section we characterized the periodic orbits of $\mathcal{G}$ and illustrated the projection of such an orbit onto the velocity plane (x_3, x_4) (see figure 3). In this and the next section we use Poincaré maps to prove that the periodic orbit is an asymptotically stable limit cycle. Several definitions are needed for the development of the results of this section. For these definitions, we denote the solution to $\mathcal{G}$ with initial condition $x_0 \in \mathcal{D}$ by $s(t, x_0), t \geq 0$. Here, $s\colon [0,\infty)\times\mathcal{D}\to\mathcal{D}$, where

$\mathcal{D} \subseteq \mathbb{R}^n$, is (i) left-continuous in t, that is, $\lim_{\tau \to t^-} s(\tau, x_0) = s(t, x_0)$ for all $x_0 \in \mathcal{D}$ and $t \in (0, \infty)$; (ii) consistent, that is, $s(0, x_0) = x_0$, for all $x_0 \in \mathcal{D}$; and (iii) satisfies the semi-group property, that is, $s(\tau, s(t, x_0)) = s(t + \tau, x_0)$ for all $x_0 \in \mathcal{D}$ and $t, \tau \in [0, \infty)$.

Definition 1: A solution $s(t, x_0)$, $t \geq 0$, of $\mathcal{G}$ is *periodic* if there exists $T > 0$ such that $s(t + T, x_0) = s(t, x_0)$ for all $t \geq 0$. The minimal $T > 0$ for which the solution $s(t, x_0)$ of $\mathcal{G}$ is periodic is called the period. A set $\mathcal{O} \subset \mathcal{D}$ is a *periodic orbit* of $\mathcal{G}$ if $\mathcal{O} = \{x \in \mathcal{D} : x = s(t, x_0), 0 \leq t \leq T\}$ for some periodic solution $s(t, x_0)$ of $\mathcal{G}$.

Definition 2: A periodic orbit $\mathcal{O}$ of $\mathcal{G}$ is *Lyapunov stable* if, for all $\epsilon > 0$, there exists $\delta = \delta(\epsilon) > 0$ such that, if $\mathrm{dist}(x_0, \mathcal{O}) < \delta$, then $\mathrm{dist}(s(t, x_0), \mathcal{O}) < \epsilon$, $t \geq 0$.

In Definition 2, $\mathrm{dist}(p, \mathcal{M})$ denotes the smallest distance from a point p to any point in the set $\mathcal{M}$; that is, $\mathrm{dist}(p, \mathcal{M}) \triangleq \inf_{x \in \mathcal{M}} \|p - x\|$.

Definition 3: A periodic orbit $\mathcal{O}$ of $\mathcal{G}$ is *asymptotically stable* if it is Lyapunov stable and there exists $\delta > 0$ such that, if $\mathrm{dist}(x_0, \mathcal{O}) < \delta$, then $\mathrm{dist}(s(t, x_0), \mathcal{O}) \to 0$ as $t \to \infty$.

The following assumptions are needed for the main result of this section:

A.1. *$f_c: \mathcal{D} \to \mathbb{R}^n$ is locally Lipschitz continuous on $\mathcal{D}$.*

A.2. *$f_d: \mathcal{S} \to \mathbb{R}^n$ is continuous.*

A.3. *There exists a continuously differentiable function $\mathcal{X}: \mathcal{D} \to \mathbb{R}$ such that the resetting set $\mathcal{S} = \{x \in \mathcal{D}: \mathcal{X}(x) = 0\}$; moreover, $\mathcal{X}'(x) \neq 0$, $x \in \mathcal{S}$.*

A.4. *$L_{f_c}\mathcal{X}(x) \triangleq \mathcal{X}'(x) f_c(x) \neq 0, x \in \mathcal{O} \cap \mathcal{S}$.*

Remark 1: It follows from A.1 and A.2 that the solution to (14) and (15) is unique and is jointly continuous in t and x_0 between resetting events (see Nersesov *et al.* (2002) for details). Hence, for any point $x_0 \in \mathcal{D}$, there exists a unique solution to (14) over a sufficiently small interval of time and the solution is continuously dependent on the initial condition. Furthermore, it follows from A.3 that the jump set $\mathcal{S}$ is an embedded submanifold (Isidori 1995) while A.2 assures that impacts vary continuously with respect to where they occur on $\mathcal{S}$. Finally, from A.4, it follows that the periodic orbit of $\mathcal{G}$ is not tangent to the jump set $\mathcal{S}$.

Next, we introduce the map $P: \mathcal{S} \to \mathcal{S}$ by

$$P(x) \triangleq s(\tau_1(x + f_d(x)),\ x + f_d(x)) \tag{44}$$

where $\tau_k(\cdot)$ denotes the kth resetting time at which $x(t)$ intersects $\mathcal{S}$. Note that it follows from A.1–A.4 that $P: \mathcal{S} \to \mathcal{S}$ is well-defined and continuous. Next, assume that at $x_0 = p \in \mathcal{S}$ the system $\mathcal{G}$ has a periodic solution such that $s(\tau_{n'}(p), p) = p$, where $\tau_{n'}(p)$ is the period. Note that $\tau_1(p) = 0$. Furthermore, define the Poincaré map $\hat{P}: \mathcal{S} \to \mathcal{S}$ by

$$\hat{P}(x) = P^{(n'-1)}(x), \qquad x \in \mathcal{S} \tag{45}$$

where $P^{(i)}(x)$ denotes the i-time composition operator of $P(x)$ with itself, $P^{(1)}(x) \triangleq P(x)$, and $n' > 1$. Hence, p is a fixed point of the discrete-time system

$$x(k+1) = \hat{P}(x(k)), \qquad k \in \overline{\mathbb{Z}}_+, \qquad x(0) \in \mathcal{S} \tag{46}$$

where $\overline{\mathbb{Z}}_+$ denotes the set of non-negative integers, and p generates a periodic orbit defined by the solution $s(t, p), t \geq 0$, of $\mathcal{G}$.

In addition to A.3, we assume, without loss of generality, that $\partial \mathcal{X}(x)/\partial x_n \neq 0, x \in \mathcal{S}$, where $x = [x_1, \ldots, x_n]^{\mathrm{T}}$. Then it follows from the implicit function theorem (Khalil 1996) that $x_n = g(x_1, \ldots, x_{n-1})$, where $g(\cdot)$ is a continuously differentiable function at $x_r \triangleq [x_1, \ldots, x_{n-1}]^{\mathrm{T}}$ such that $[x_r^{\mathrm{T}}, g(x_r)]^{\mathrm{T}} \in \mathcal{S}$. Note that in this case $\hat{P}: \mathcal{S} \to \mathcal{S}$ in (46) is given by $\hat{P}(x) \triangleq [\hat{P}_1(x), \ldots, \hat{P}_n(x)]^{\mathrm{T}}$, where

$$\hat{P}_n(x_r, g(x_r)) = g(\hat{P}_1(x_r, g(x_r)), \ldots, \hat{P}_{n-1}(x_r, g(x_r))) \tag{47}$$

Hence, we can reduce the n-dimensional system (46) to the $(n-1)$-dimensional system

$$x_r(k+1) = \mathcal{P}_r(x_r(k)), \qquad k \in \overline{\mathbb{Z}}_+ \tag{48}$$

where $x_r \in \mathbb{R}^{n-1}$, $[x_r^{\mathrm{T}}(\cdot),\ g(x_r(\cdot))]^{\mathrm{T}} \in \mathcal{S}$, and

$$\mathcal{P}_r(x_r) \triangleq \begin{bmatrix} \hat{P}_1(x_r, g(x_r)) \\ \vdots \\ \hat{P}_{n-1}(x_r, g(x_r)) \end{bmatrix} \tag{49}$$

Note that it follows from (47) and (49) that $x_0 \triangleq [x_{0r}^{\mathrm{T}}, g(x_{0r})]^{\mathrm{T}} \in \mathcal{S}$ is a fixed point of (46) if and only if x_{0r} is a fixed point of (48).

The following theorem given in Nersesov *et al.* (2002) generalizes Poincaré's theorem to impulsive dynamical systems by establishing a relationship between the stability properties of the periodic orbit $\mathcal{O}$ and the stability properties of an equilibrium point of the discrete-time system (48). A related result is given in Grizzle *et al.* (2001).

Theorem 1 (Nersesov *et al.* 2002)**:** *Consider the nonlinear impulsive dynamical system $\mathcal{G}$ with the Poincaré map defined by* (45) *and let $x_0 = [x_{r0}^{\mathrm{T}}, g(x_{r0})]^{\mathrm{T}} \in \mathcal{S}$. Assume that A.1–A.4 hold and $\partial \mathcal{X}(x)/\partial x_n \neq 0, x \in \mathcal{S}$. Then the following statements hold:*

(i) x_{r0} *is a Lyapunov stable fixed point of* (48) *if and only if the periodic orbit* $\mathcal{O}$ *generated by* $x_0 \in \mathcal{S}$ *is Lyapunov stable.*

(ii) x_{r0} *is an asymptotically stable fixed point of* (48) *if and only if the periodic orbit* $\mathcal{O}$ *generated by* $x_0 \in \mathcal{S}$ *is asymptotically stable.*

6. Limit cycle analysis of the clock escapement mechanism

In this section we use Theorem 1 to show that the periodic orbit generated by the escapement mechanism is asymptotically stable. For convenience we denote the periodic orbit values of $\dot{\theta}_{c1}$, $\dot{\theta}_{c0}$ and $\dot{\theta}_v$ given by (41), (40) and (42) by a, b and $\pm c$, respectively. The following assumption is needed.

Assumption 1: $\alpha_v < \pi/2$.

It follows from (37) that between consecutive collisions *on the periodic orbit*, the mean line of the angular offset between two paddles sweeps an angle of α_v, that is, $\alpha_v = c\Delta t$. This assures the existence of a fixed point of (48) for the escapement mechanism. Furthermore, Assumption 1 assures that $\mathcal{X}: \mathcal{D} \to \mathbb{R}$ is continuously differentiable. To see this, note that $\mathcal{X}(\cdot)$ is determined by (21) and (22). Now, in order for $\mathcal{X}(\cdot)$ to be continuously differentiable we need to avoid $x_2 + (\alpha_v/2) = \pm\pi/2$ and $-x_2 + (\alpha_v/2) = \pm\pi/2$. Since the position of the verge is always within the range $(-(\alpha_v/2) - \epsilon, (\alpha_v/2) + \epsilon)$, where $\epsilon > 0$ is small, it follows that in order to avoid the singularity $\pm\pi/2$ we need to make sure that $\alpha_v + \epsilon \neq \pi/2$ which can be achieved by assuming $\alpha_v < \pi/2$.

Without loss of generality, suppose that the trajectory $s(t, x_0)$, $t \geq 0$, of $\mathcal{G}$ starts from a point in the four-dimensional state space associated with the upper paddle collision such that its projection onto the three-dimensional subspace lies in a sufficiently small neighbourhood of the point $(x_2, x_3, x_4) = (-\alpha_v/2, b, -c)$. Then, we can construct a three-dimensional discrete-time system that identifies the next point (x_2, x_3, x_4) on the trajectory right before the next upper paddle collision. This iterative procedure can be captured by the non-linear difference equation

$$\begin{bmatrix} x_2(k+1) \\ x_3(k+1) \\ x_4(k+1) \end{bmatrix} = \begin{bmatrix} f_2(x_2(k),\, x_3(k),\, x_4(k)) \\ f_3(x_2(k),\, x_3(k),\, x_4(k)) \\ f_4(x_2(k),\, x_3(k),\, x_4(k)) \end{bmatrix} \tag{50}$$

where $f_2(\cdot,\cdot,\cdot), f_3(\cdot,\cdot,\cdot)$, and $f_4(\cdot,\cdot,\cdot)$ are given in Appendix A. It follows from (35)–(37) that the point $(-(\alpha_v/2), b, -c)$ is a fixed point of (50). Next, it follows from standard discrete-time stability theory that if $\rho(J(-\alpha_v/2, b, -c)) < 1$, where (see bottom of page)

and $\rho(\cdot)$ denotes spectral radius, then the point $(x_2, x_3, x_4) = (-\alpha_v/2, b, -c)$ is a locally asymptotically stable fixed point of (50).

Next, we introduce the discrete-time dynamical system

$$\begin{bmatrix} \hat{x}_2(k+1) \\ \hat{x}_3(k+1) \\ \hat{x}_4(k+1) \end{bmatrix} = \begin{bmatrix} f_2^{(n)}(\hat{x}_2(k), \hat{x}_3(k), \hat{x}_4(k)) \\ f_3^{(n)}(\hat{x}_2(k), \hat{x}_3(k), \hat{x}_4(k)) \\ f_4^{(n)}(\hat{x}_2(k), \hat{x}_3(k), \hat{x}_4(k)) \end{bmatrix} \tag{52}$$

where $f_i^{(n)}(\hat{x}_2(k), \hat{x}_3(k), \hat{x}_4(k)), i = 2, 3, 4$, denotes the n-time composition operator of $f_i(\cdot,\cdot,\cdot)$, $i = 2, 3, 4$, with $f_2(\cdot,\cdot,\cdot)$, $f_3(\cdot,\cdot,\cdot)$, and $f_4(\cdot,\cdot,\cdot)$ and n is the number of the crown gear teeth. Note that $(\hat{x}_2, \hat{x}_3, \hat{x}_4) = (-\alpha_v/2, b, -c)$ is a fixed point of (52).

Proposition 1: *Consider the impulsive dynamical system* $\mathcal{G}$. *If* $\rho(J(-\alpha_v/2, b, -c)) < 1$, *then the point* $(\hat{x}_2, \hat{x}_3, \hat{x}_4) = (-\alpha_v/2, b, -c)$ *is a locally asymptotically stable fixed point of* (52). *Alternatively, if* $\rho(J(-\alpha_v/2, b, -c)) > 1$, *then the fixed point* $(-\frac{\alpha_v}{2}, b, -c)$ *of* (52) *is unstable.*

Proof: Given a continuously differentiable function $f: \mathbb{R}^n \to \mathbb{R}^n$, consider the N-time composition operator of $f(\cdot)$ with itself; that is, $h(x) \triangleq f^{(N)}(x)$, $x \in \mathbb{R}^n$, $N \in \overline{\mathbb{Z}}_+$. Now, using the chain rule for vector valued functions it follows that

$$\frac{\partial h(x)}{\partial x} = \left.\frac{\partial f(s_1)}{\partial s_1}\right|_{s_1 = f^{(N-1)}(x)} \cdot \left.\frac{\partial f(s_2)}{\partial s_2}\right|_{s_2 = f^{(N-2)}(x)} \cdot \cdots \cdot \left.\frac{\partial f(s_N)}{\partial s_N}\right|_{s_N = f^0(x)}, \quad x \in \mathbb{R}^n \tag{53}$$

where $f^0(x) \triangleq x$. Next, since $(-\alpha_v/2, b, -c)$ is a fixed point of the system (50), it follows that the Jacobian matrix $\hat{J}(\hat{x}_2(k), \hat{x}_3(k), \hat{x}_4(k))$ of the discrete-time system

$$J\left(-\frac{\alpha_v}{2}, b, -c\right) \triangleq \left.\begin{bmatrix} \dfrac{\partial f_2(x_2,x_3,x_4)}{\partial x_2} & \dfrac{\partial f_2(x_2,x_3,x_4)}{\partial x_3} & \dfrac{\partial f_2(x_2,x_3,x_4)}{\partial x_4} \\ \dfrac{\partial f_3(x_2,x_3,x_4)}{\partial x_2} & \dfrac{\partial f_3(x_2,x_3,x_4)}{\partial x_3} & \dfrac{\partial f_3(x_2,x_3,x_4)}{\partial x_4} \\ \dfrac{\partial f_4(x_2,x_3,x_4)}{\partial x_2} & \dfrac{\partial f_4(x_2,x_3,x_4)}{\partial x_3} & \dfrac{\partial f_4(x_2,x_3,x_4)}{\partial x_4} \end{bmatrix}\right|_{(x_2,x_3,x_4)=(-\alpha_v/2,b,-c)} \tag{51}$$

(52) evaluated at the fixed point $(-\alpha_v/2, b, -c)$ is given by the N-time product of $J(-\alpha_v/2, b, -c)$; that is

$$\hat{\boldsymbol{J}}\left(-\frac{\alpha_v}{2}, b, -c\right) = J^N\left(-\frac{\alpha_v}{2}, b, -c\right) \tag{54}$$

Hence

$$\rho\left(\hat{\boldsymbol{J}}\left(-\frac{\alpha_v}{2}, b, -c\right)\right) = \rho^N\left(J\left(-\frac{\alpha_v}{2}, b, -c\right)\right) \tag{55}$$

Now, it follows that if $\rho(J(-\alpha_v/2, b, -c)) < 1$, then $\rho(\hat{\boldsymbol{J}}(-\alpha_v/2, b, -c)) < 1$, which implies that $(-\alpha_v/2, b, -c)$ is a locally asymptotically stable fixed point of (52). Alternatively, if $\rho(J(-\alpha_v/2, b, -c)) > 1$, then $\rho(\hat{\boldsymbol{J}}(-\alpha_v/2, b, -c)) > 1$, which implies that the fixed point $(-\alpha_v/2, b, -c)$ of (52) is unstable. □

Next, it follows from the uniqueness of solutions of $\mathcal{G}$ and the fact that the initial conditions (x_1', x_2, x_3, x_4) and (x_1, x_2, x_3, x_4), where $x_1 = x_1' + 2\pi$, give rise to identical solutions for $\mathcal{G}$, that the point $x_0 = (0, -\alpha_v/2, b, -c)$ is a fixed point for the discrete-time system capturing the state of $\mathcal{G}$ immediately before every $(np+1)$th upper paddle collision for $p = 0, 1, 2, \ldots$. Note that whenever an upper paddle collision occurs, the position of the crown gear is completely defined by the position of the verge, and the relation between them results from the collision condition; that is, $x_1 = f_1(x_2)$, where $f_1 : \mathbb{R} \to \mathbb{R}$ is defined by (21). Thus, the aforementioned four-dimensional system has the form

$$\begin{bmatrix} \tilde{x}_1(k+1) \\ \tilde{x}_2(k+1) \\ \tilde{x}_3(k+1) \\ \tilde{x}_4(k+1) \end{bmatrix} = \begin{bmatrix} f_1(f_2^{(n)}(\tilde{x}_2(k), \tilde{x}_3(k), \tilde{x}_4(k))) \\ f_2^{(n)}(\tilde{x}_2(k), \tilde{x}_3(k), \tilde{x}_4(k)) \\ f_3^{(n)}(\tilde{x}_2(k), \tilde{x}_3(k), \tilde{x}_4(k)) \\ f_4^{(n)}(\tilde{x}_2(k), \tilde{x}_3(k), \tilde{x}_4(k)) \end{bmatrix} \tag{56}$$

where $f_1(\cdot)$ is given by

$$f_1(x_2) = \arcsin\left(\frac{r_v}{r_c}\tan\left(x_2 + \frac{\alpha_v}{2}\right)\right) \tag{57}$$

Next, we identify the periodic orbit generated by the point $x_0 = (0, -\alpha_v/2, b, -c)$. For any point on this orbit with $(x_3, x_4) = (z, c), z \in (a, b]$, it follows that $z = a + (\tau/I_c)t_z$, where t_z is time spanned for the crown gear to restore its velocity from the value of a to z. Thus, this point can be characterized as

$$x_z = \begin{bmatrix} x_{10} + \dfrac{a(z-a)}{\tau}I_c + \dfrac{(z-a)^2}{2\tau}I_c \\ -\dfrac{\alpha_v}{2} + \dfrac{c(z-a)}{\tau}I_c \\ z \\ c \end{bmatrix} \tag{58}$$

where $x_{10} = l\alpha_c, l = 0, 1, 2, \ldots, n-1$. Similarly, every point on the orbit with $(x_3, x_4) = (z, -c), z \in (a, b]$, is characterized as

$$x_z' = \begin{bmatrix} x_{10}' + \frac{a(z-a)}{\tau}I_c + \frac{(z-a)^2}{2\tau}I_c \\ \frac{\alpha_v}{2} - \frac{c(z-a)}{\tau}I_c \\ z \\ -c \end{bmatrix} \tag{59}$$

where $x_{10}' = ((2l+1)/2)\alpha_c, l = 0, 1, 2, ..., n-1$. Since the initial conditions (x_1', x_2, x_3, x_4) and (x_1, x_2, x_3, x_4), where $x_1 = x_1' + 2\pi$, give rise to identical solutions for $\mathcal{G}$, it follows that $\mathcal{O} \triangleq \{y \in \mathbb{R}^4 : y = x_z\} \cup \{y \in \mathbb{R}^4 : y = x_z'\}$ is the periodic orbit of $\mathcal{G}$. The expressions given by (58) and (59) imply that points $x_0 = (x_{10}, -\alpha_v/2, b, -c) \in \mathcal{S}$ or $x_0 = (x_{10}', \alpha_v/2, b, c) \in \mathcal{S}$ generate $\mathcal{O}$. Next, we show that $\mathcal{O}$ is locally asymptotically stable. For this result let $\mathcal{D}$ be a sufficiently small neighbourhood of $\mathcal{O}$ for which the state of $\mathcal{G}$ is defined.

Theorem 2: *Consider the impulsive dynamical system $\mathcal{G}$. Then the following statements hold:*

(i) *If $\rho(J(-\alpha_v/2, b, -c)) < 1$, then the periodic orbit $\mathcal{O}$ of $\mathcal{G}$ generated by $x_0 = (x_{10}, -\alpha_v/2, b, -c) \in \mathcal{S}$ or $x_0 = (x_{10}', \alpha_v/2, b, c) \in \mathcal{S}$ is locally asymptotically stable.*

(ii) *If $\rho(J(-\alpha_v/2, b, -c)) > 1$, then the periodic orbit $\mathcal{O}$ of $\mathcal{G}$ generated by $x_0 = (x_{10}, -\alpha_v/2, b, -c) \in \mathcal{S}$ or $x_0 = (x_{10}', \alpha_v/2, b, c) \in \mathcal{S}$ is unstable.*

Proof: First we show that A.1–A.4 hold for $\mathcal{G}$. Assumptions A.1 and A.2 are immediately satisfied for $\mathcal{G}$. To see that A.3 holds, note that for $\mathcal{S}_m^{\text{upper}}$ given by (21) with a small angle approximation, $\mathcal{X}'(x) = [r_c, -r_v, 0, 0] \neq 0$, $x \in \mathcal{S}_m^{\text{upper}}$, and $\partial\mathcal{X}(x)/\partial x_1 \neq 0$, $x \in \mathcal{S}_m^{\text{upper}}$. Furthermore, for $\mathcal{S}_m^{\text{lower}}$ given by (22) with a small angle approximation, $\mathcal{X}'(x) = [r_c, r_v, 0, 0] \neq 0$, $x \in \mathcal{S}_m^{\text{lower}}$, and $\partial\mathcal{X}(x)/\partial x_1 \neq 0, x \in \mathcal{S}_m^{\text{lower}}$. Note, that in both cases $\mathcal{X}(\cdot)$ is a continuously differentiable function by Assumption 1. To see that A.4 holds, note that $L_{f_c}\mathcal{X}(x) = r_c x_3 - r_v x_4 > 0$, $x \in \mathcal{S}_m^{\text{upper}}$, and $L_{f_c}\mathcal{X}(x) = r_c x_3 + r_v x_4 > 0$, $x \in \mathcal{S}_m^{\text{lower}}$. Next, to show (i) assume that $\rho(J(-\alpha_v/2, b, -c)) < 1$. Then it follows from Proposition 1 that the fixed point $(-\alpha_v/2, b, -c)$ of (52) is locally asymptotically stable and by Theorem 1 the periodic orbit $\mathcal{O}$ of $\mathcal{G}$ is locally asymptotically stable. Finally, the proof to (ii) follows analogously.

The condition $\rho(J(-\alpha_v/2, b, -c)) < 1$ guarantees local asymptotic stability of the escapement mechanism. Alternatively, it follows from physical considerations that for each choice of clock parameters, if the value of the coefficient of restitution e is sufficiently close to 1, then the escapement mechanism dissipates less energy

during a collision event than it gains from the rotational torque between collisions. This leads to instability of the mechanism. However, the Jacobian matrix J is sufficiently complex that we have been unable to show analytically the explicit dependence of the spectral radius of J on the parameter e.

7. Numerical example

In this section we numerically integrate the equations of motion (17)–(22) to illustrate convergence of the trajectories to a limit cycle. We choose the parameters $\tau = 1\ \mathrm{N}\cdot\mathrm{m}$, $e = 0.05$, $I_c = 10\ \mathrm{kg}\cdot\mathrm{m}^2$, $I_v = 0.15\ \mathrm{kg}\cdot\mathrm{m}^2$, $r_c = 1$ m, $r_v = 0.3$ m and $\alpha_c = 24$ deg. For these parameters it follows from (39)–(43) that the periodic orbit has an average crown gear velocity of 0.257 rad/s, a crown gear velocity of 0.297 rad/s prior to collisions, a crown gear velocity of 0.216 rad/s after collisions, a verge speed of 0.813 rad/s, and a period of 1.63 sec. Furthermore, the eigenvalues of the Jacobian matrix (51) are $\lambda_1 = -0.7191$, $\lambda_2 = 0.2072$, and $\lambda_3 = -0.0149$, which implies that the fixed point $(-\alpha_v/2, b, -c)$ of (52) is locally asymptotically stable and hence by Theorem 2 the periodic orbit of the escapement mechanism is asymptotically stable. An initial verge position of $\theta_{v_0} = 0$ is chosen for all simulations. We assume that the verge and the crown gear are in contact at the start of the simulation, which determines the crown gear's initial position.

For a collection of four initial conditions, Figure 5 shows the trajectories of the system in terms of the verge and crown gear velocities $\dot{\theta}_v$ and $\dot{\theta}_c$. For each choice of initial conditions it can be seen that the trajectory approaches a periodic orbit, which is discontinuous due to the impulsive nature of the collisions. Numerical computation of the amplitude and period of this orbit from the simulation data yields 0.257 rad/s and 1.63 s, respectively, which agrees with the values given by (39) and (43).

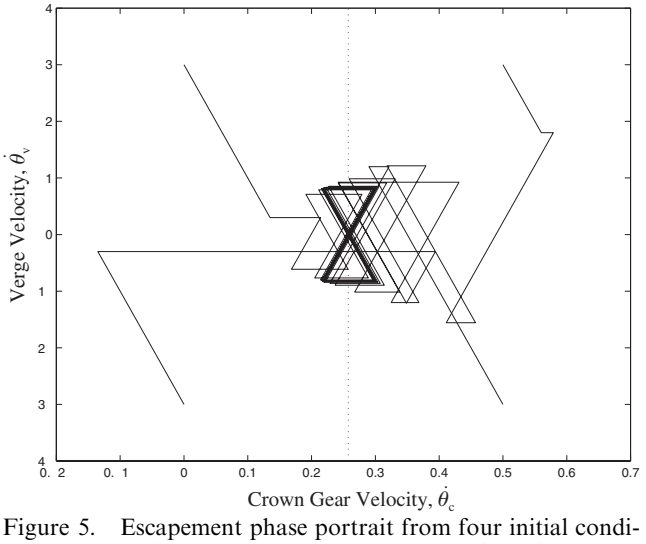

Figure 5. Escapement phase portrait from four initial conditions showing convergence to a periodic orbit. Initial conditions are $(\dot{\theta}_c, \dot{\theta}_v) = (0.5, 3)$, $(0.5, -3)$, $(0, 3)$, and $(0, -3)$. The average crown gear velocity from (39) is plotted with a dotted line.

The kinetic energy time histories of the verge, crown gear, and total system are shown in figure 6 for the system considered in figure 5. It can be seen that the verge kinetic energy converges, whereas the crown gear and total system kinetic energies converge to periodic signals.

For two values of the coefficient of restitution, figure 7 shows the time history of the crown gear velocity $\dot{\theta}_c$ as it approaches the periodic orbit given by (39) and (43). The average velocity and orbit period are 0.2449 rad/s and 1.7104 s, respectively, for $e = 0.1$, and 0.1354 rad/s and 3.0942 s, respectively, for $e = 0.6$. A full orbit cycle appears as two consecutive saw-tooth patterns in figure 7.

Finally, instability of the escapement mechanism implies that the escapement mechanism gains more energy from the rotational torque between collisions than it loses during collisions. To illustrate that $\rho(J(-\alpha_v/2, b, -c)) > 1$ leads to an unstable limit cycle, let $\tau = 10\ \mathrm{N}\cdot\mathrm{m}$, $e = 0.05$, $I_c = 7\ \mathrm{kg}\cdot\mathrm{m}^2$, $I_v =$

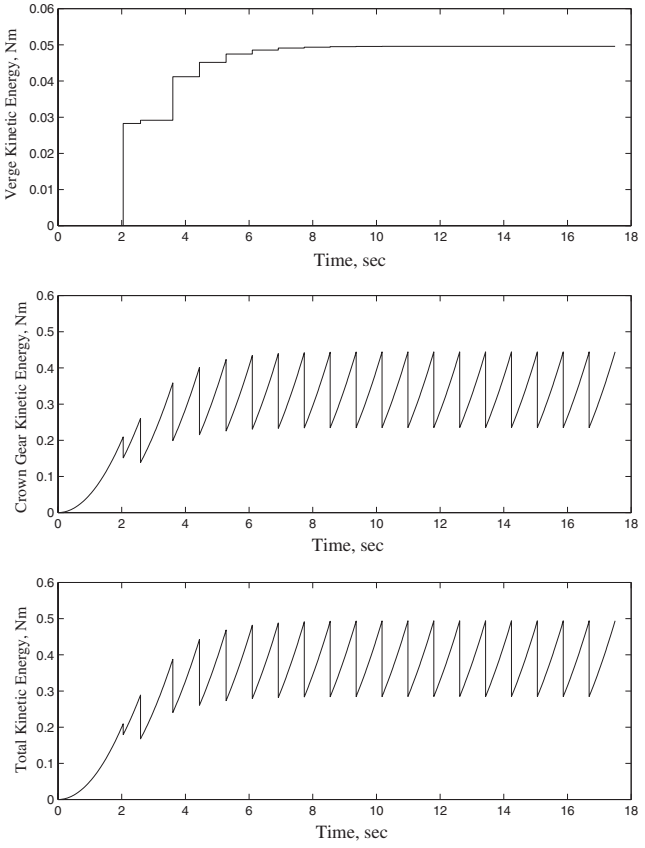

Figure 6. Verge, crown gear, and total kinetic energy time histories starting from rest.

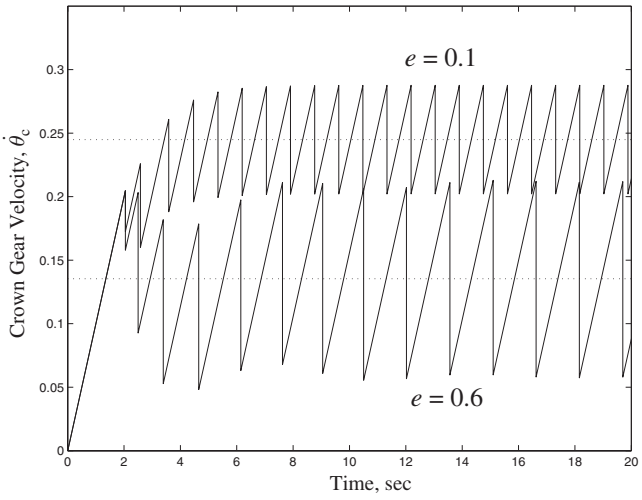

Figure 7. Time histories of the crown gear velocity $\dot{\theta}_c$ starting from rest with coefficients of restitution of 0.1 and 0.6. The values of $\overline{\dot{\theta}_c}$ from (39) are plotted as dotted lines.

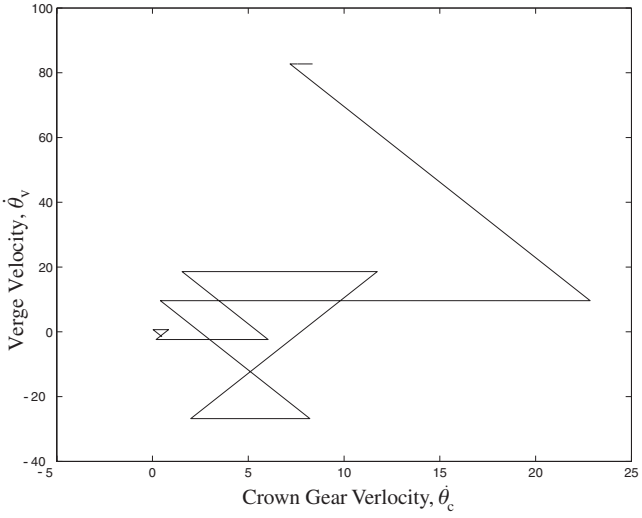

Figure 8. Velocity phase portrait for the unstable escapement.

0.15 kg · m^2, $r_c = 3$ m, $r_v = 0.3$ m and $\alpha_c = 24$ deg, so that the eigenvalues of the Jacobian matrix (51) are $\lambda_1 = 1.8559$, $\lambda_2 = 0.1775$ and $\lambda_3 = 0.0046$. Since the fixed point $(-\alpha_v/2, b, -c)$ of the discrete-time system (52) is unstable, it follows from theorem 2 that the periodic orbit of the escapement mechanism is also unstable. Figure 8 shows the non-converging velocity phase portrait of the system. Finally, figure 9 shows $\rho(J(-\alpha_v/2, b, -c))$ versus the coefficient of restitution e for several values of the torque τ.

8. Conclusion

In this paper we derived the equations of motion for a verge and foliot escapement mechanism, which is a mechanical regulator in which feedback occurs through mechanical collisions. We showed that an impulsive differential equation can be used to model the continuous and impulsive dynamics of this system. Using conservation of momentum and accounting for energy lost during collisions, we obtained analytical expressions for the period and crown gear angular velocity of a periodic orbit of the system. Furthermore, using Poincaré maps for impulsive dynamical systems we showed that the resulting periodic orbits are locally asymptotically stable.

Finally, the model of the verge and foliot clock developed and analysed in this paper includes the dynamics of the clock under a simplified model of collision and contact. In particular, the collision model is a simple restitution law, while the model does not include sliding contact and associated friction that generally occurs in a real clock when the pallets are in contact with the teeth. While a more realistic treatment of these effects is outside the scope of this paper, we expect minimal impact on the existence and nature of limit cycles.

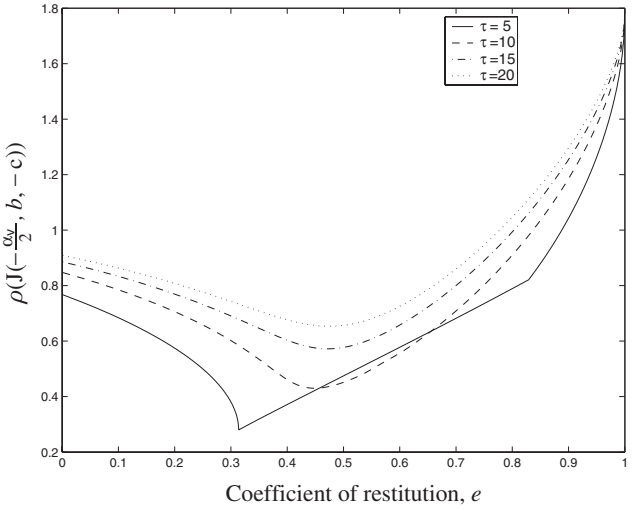

Figure 9. $\rho(J(-\alpha_v/2, b, -c))$ versus coefficient of restitution for different values of torque τ.

Acknowledgements

This research was supported in part by the Air Force Office of Scientific Research under Grants F49620-98-1-0037 and F49620-00-1-0095, the National Science Foundation under Grant ECS-94624, and a François Xavier Bagnoud Foundation Fellowship.

Appendix

The purpose of this Appendix is to characterize the functions $f_2(x_2(k), x_3(k), x_4(k))$, $f_3(x_2(k), x_3(k), x_4(k))$

and $f_4(x_2(k), x_3(k), x_4(k))$ given in (50). For this analysis we denote the intermediate states of $\mathcal{G}$ between two consecutive upper paddle collisions as follows: (x_1', x_2', x_3', x_4') denotes the state of $\mathcal{G}$ immediately after the upper paddle collision, $(x_1'', x_2'', x_3'', x_4'')$ denotes the state of $\mathcal{G}$ immediately before the lower paddle collision and $(x'''_1, x'''_2, x'''_3, x'''_4)$ denotes the state of $\mathcal{G}$ immediately after the lower paddle collision. Hence, using (18), the next point immediately after the initial upper paddle collision is given by

$$\begin{bmatrix} x_2'(k) \\ x_3'(k) \\ x_4'(k) \end{bmatrix} = \begin{bmatrix} 0 & 0 & 0 \\ 0 & -r_c G_c & r_v G_c \\ 0 & r_c G_v & -r_v G_v \end{bmatrix} \begin{bmatrix} x_2(k) \\ x_3(k) \\ x_4(k) \end{bmatrix} + \begin{bmatrix} x_2(k) \\ x_3(k) \\ x_4(k) \end{bmatrix} \tag{60}$$

Since the verge moves with constant velocity and the crown gear moves with acceleration τ/I_c on the continuous part of the trajectory, the next intermediate point immediately before the lower paddle collision is given by

$$\begin{bmatrix} x_2''(k) \\ x_3''(k) \\ x_4''(k) \end{bmatrix} = \begin{bmatrix} x_2'(k) \\ x_3'(k) \\ x_4'(k) \end{bmatrix} + \begin{bmatrix} x_4'(k)\Delta t_1(x_2(k), x_3(k), x_4(k)) \\ (\tau/I_c)\Delta t_1(x_2(k), x_3(k), x_4(k)) \\ 0 \end{bmatrix} \tag{61}$$

where $\Delta t_1(x_2(k), x_3(k), x_4(k))$ is the time between successive collisions of the upper and lower paddles, respectively. Similarly, using (18), the next intermediate point immediately after the lower paddle collision is given by

$$\begin{bmatrix} x'''_2(k) \\ x'''_3(k) \\ x'''_4(k) \end{bmatrix} = \begin{bmatrix} 0 & 0 & 0 \\ 0 & -r_c G_c & -r_v G_c \\ 0 & -r_c G_v & -r_v G_v \end{bmatrix} \begin{bmatrix} x_2''(k) \\ x_3''(k) \\ x_4''(k) \end{bmatrix} + \begin{bmatrix} x_2''(k) \\ x_3''(k) \\ x_4''(k) \end{bmatrix} \tag{62}$$

Hence

$$\begin{bmatrix} x_2(k+1) \\ x_3(k+1) \\ x_4(k+1) \end{bmatrix} = \begin{bmatrix} x'''_2(k) \\ x'''_3(k) \\ x'''_4(k) \end{bmatrix} + \begin{bmatrix} x'''_4(k)\Delta t_2((x_2(k), x_3(k), x_4(k)) \\ (\tau/I_c)\Delta t_2((x_2(k), x_3(k), x_4(k)) \\ 0 \end{bmatrix} \tag{63}$$

is the state of (50) associated with the instant immediately before the next upper paddle collision, where $\Delta t_2(x_2(k), x_3(k), x_4(k))$ is the time between successive collisions of the lower and upper paddles, respectively. Now, using (60)–(63) we obtain

$$\begin{aligned} \begin{bmatrix} x_2(k+1) \\ x_3(k+1) \\ x_4(k+1) \end{bmatrix} &= A \begin{bmatrix} x_2(k) \\ x_3(k) \\ x_4(k) \end{bmatrix} \\ &+ \begin{bmatrix} 0 & 0 & 0 \\ 0 & -r_c G_c & -r_v G_c \\ 0 & -r_c G_v & -r_v G_v \end{bmatrix} \\ &\times \begin{bmatrix} x_4'(k)\Delta t_1(x_2(k), x_3(k), x_4(k)) \\ (\tau/I_c)\Delta t_1(x_2(k), x_3(k), x_4(k)) \\ 0 \end{bmatrix} \\ &+ \begin{bmatrix} 1 & 0 & 0 \\ 0 & 1 & 0 \\ 0 & 0 & 1 \end{bmatrix} \\ &\times \begin{bmatrix} x_4'(k)\Delta t_1(x_2(k), x_3(k), x_4(k)) \\ (\tau/I_c)\Delta t_1(x_2(k), x_3(k), x_4(k)) \\ 0 \end{bmatrix} \\ &+ \begin{bmatrix} x'''_4(k)\Delta t_2(x_2(k), x_3(k), x_4(k)) \\ (\tau/I_c)\Delta t_2(x_2(k), x_3(k), x_4(k)) \\ 0 \end{bmatrix} \end{aligned} \tag{64}$$

where

$$\begin{aligned} A = &\begin{bmatrix} 0 & 0 & 0 \\ 0 & -r_c G_c & -r_v G_c \\ 0 & -r_c G_v & -r_v G_v \end{bmatrix} \begin{bmatrix} 0 & 0 & 0 \\ 0 & -r_c G_c & r_v G_c \\ 0 & r_c G_v & -r_v G_v \end{bmatrix} \\ &+ \begin{bmatrix} 0 & 0 & 0 \\ 0 & -r_c G_c & -r_v G_c \\ 0 & -r_c G_v & -r_v G_v \end{bmatrix} \\ &+ \begin{bmatrix} 0 & 0 & 0 \\ 0 & -r_c G_c & r_v G_c \\ 0 & r_c G_v & -r_v G_v \end{bmatrix} + \begin{bmatrix} 1 & 0 & 0 \\ 0 & 1 & 0 \\ 0 & 0 & 1 \end{bmatrix} \end{aligned} \tag{65}$$

Next, we compute $\Delta t_1(x_2(k), x_3(k), x_4(k))$ and $\Delta t_2(x_2(k), x_3(k), x_4(k))$ as in § 4. Specifically, integrating the continuous-time dynamics after the upper paddle collision we obtain

$$x_1''(k) = x_1(k) + x_3'(k)\Delta t_1 + \frac{\tau}{2I_c}\Delta t_1^2 \tag{66}$$

$$x_2''(k) = x_2(k) + x_4'(k)\Delta t_1 \tag{67}$$

where $x_1(k)$ is the position of the crown gear immediately before the initial upper paddle collision. Using (21) the condition for the initial collision involving the upper paddle is

$$r_c \sin(x_1(k) - m\alpha_c) = r_v \tan\left(x_2(k) + \frac{\alpha_v}{2}\right) \tag{68}$$

where m is the index of the crown gear tooth involved in the collision. Furthermore, using (26), (27), (66) and (67) yields

$$r_c \sin\left(-x_1(k) - x_3'(k)\Delta t_1 - \frac{\tau}{2I_c}\Delta t_1^2 + m\alpha_c + \pi + \frac{\alpha_c}{2}\right) = r_v \tan\left(-x_2(k) - x_4'(k)\Delta t_1 + \frac{\alpha_v}{2}\right) \tag{69}$$

Since $\sin(\pi - \alpha) = \sin\alpha$ and, for small angles, $\sin\alpha \approx \alpha$, we can rewrite (68) and (69) as

$$r_c(x_1(k) - m\alpha_c) = r_v\left(x_2(k) + \frac{\alpha_v}{2}\right) \tag{70}$$

$$r_c\left(x_1(k) + x_3'(k)\Delta t_1 + \frac{\tau}{2I_c}\Delta t_1^2 - m\alpha_c - \frac{\alpha_c}{2}\right) = r_v\left(-x_2(k) - x_4'(k)\Delta t_1 + \frac{\alpha_v}{2}\right) \tag{71}$$

Subtracting (71) from (70) yields

$$\frac{r_c\tau}{2I_c}\Delta t_1^2 + (r_c x_3'(k) + r_v x_4'(k))\Delta t_1 + 2r_v x_2(k) - \frac{r_c\alpha_c}{2} = 0 \tag{72}$$

which further implies (see (73) bottom of page)
Using (60) it follows that

$$\begin{aligned} r_c x_3'(k) + r_v x_4'(k) &= r_c(-r_c G_c x_3(k) + r_v G_c x_4(k) + x_3(k)) \\ &\quad + r_v(r_c G_v x_3(k) - r_v G_v x_4(k) + x_4(k)) \\ &= (-r_c^2 G_c + r_c + r_v r_c G_v) x_3(k) \\ &\quad + (-r_v^2 G_v + r_v + r_c r_v G_c) x_4(k) \\ &= -\alpha x_3(k) - \beta x_4(k) \end{aligned} \tag{74}$$

where

$$\begin{aligned} \alpha &= -(-r_c^2 G_c + r_c + r_v r_c G_v), \\ \beta &= -(-r_v^2 G_v + r_v + r_c r_v G_c) \end{aligned} \tag{75}$$

Thus, we obtain

$$\Delta t_1(x_2(k), x_3(k), x_4(k)) = \frac{\alpha x_3(k) + \beta x_4(k) + \sqrt{(\alpha x_3(k) + \beta x_4(k))^2 + \lambda}}{r_c\tau/I_c} \tag{76}$$

where $\lambda \triangleq \lambda(x_2(k)) = (r_c\tau/I_c)(r_c\alpha_c - 4r_v x_2(k))$. Next, it follows from (62) that $x'''_3(k)$ and $x'''_4(k)$ are the velocities of the crown gear and the verge, respectively, immediately after the lower paddle collision, and hence the positions of the crown gear and the verge before the successive upper paddle collision are given by

$$\left.\begin{aligned} x_1(k+1) &= x'''_1(k) + x'''_3(k)\Delta t_2 + \frac{\tau}{2I_c}\Delta t_2^2 \\ x_2(k+1) &= x'''_2(k) + x'''_4(k)\Delta t_2 \end{aligned}\right\} \tag{77}$$

where $x'''_1(k)$ and $x'''_2(k)$ are positions of the crown gear and the verge, respectively, immediately after the lower paddle collision. Using a similar procedure as outlined above, the conditions for the lower and upper paddle collisions, respectively, are given by

$$r_c \sin\left(m\alpha_c + \pi + \frac{\alpha_c}{2} - x'''_1(k)\right) = r_v \tan\left(-x'''_2(k) + \frac{\alpha_v}{2}\right)$$

$$r_c \sin\left(x'''_1(k) + x'''_3(k)\Delta t_2 + \frac{\tau}{2I_c}\Delta t_2^2 - (m+1)\alpha_c\right) = r_v \tan\left(x'''_2(k) + x'''_4(k)\Delta t_2 + \frac{\alpha_v}{2}\right)$$

which can be approximated by

$$r_c\left(x'''_1(k) - m\alpha_c - \frac{\alpha_c}{2}\right) = r_v\left(-x'''_2(k) + \frac{\alpha_v}{2}\right) \tag{78}$$

$$r_c\left(x'''_1(k) + x'''_3(k)\Delta t_2 + \frac{\tau}{2I_c}\Delta t_2^2 - (m+1)\alpha_c\right) = r_v\left(x'''_2(k) + x'''_4(k)\Delta t_2 + \frac{\alpha_v}{2}\right) \tag{79}$$

Subtracting (79) from (78) gives

$$\frac{r_c\tau}{2I_c}\Delta t_2^2 + (r_c x'''_3(k) - r_v x'''_4(k))\Delta t_2 - \frac{r_c\alpha_c}{2} - 2r_v x'''_2(k) = 0$$

so that (see (80) bottom of page)

From (60)–(62), and (76) it follows that

$$\Delta t_1 = \frac{-(r_c x_3'(k) + r_v x_4'(k)) + \sqrt{(r_c x_3'(k) + r_v x_4'(k))^2 + (r_c\tau/I_c)(r_c\alpha_c - 4r_v x_2(k))}}{r_c\tau/I_c} \tag{73}$$

$$\Delta t_2 = \frac{-(r_c x'''_3(k) - r_v x'''_4(k)) + \sqrt{(r_c x'''_3(k) - r_v x'''_4(k))^2 + (r_c\tau/I_c)(r_c\alpha_c + 4r_v x'''_2(k))}}{r_c\tau/I_c} \tag{80}$$

$$x'''_3(k) = \left((-r_cG_c+1)^2 - r_vG_cr_cG_v + \alpha(-G_c+\frac{1}{r_c})\right)x_3(k) + \left(r_vG_c(-r_cG_c+1) + r_v^2G_vG_c - r_vG_c + \beta(-G_c+\frac{1}{r_c})\right)x_4(k) + \left(-G_c+\frac{1}{r_c}\right)\sqrt{(\alpha x_3(k)+\beta x_4(k))^2+\lambda} \quad (81)$$

Similarly, from (60)–(62) and (76) it follows that

$$x'''_4(k) = (r_c^2G_cG_v - r_cG_v + (-r_vG_v+1)r_cG_v - \alpha G_v)x_3(k) + (-r_cG_vr_vG_c + (-r_vG_v+1)^2 - \beta G_v)x_4(k) - G_v\sqrt{(\alpha x_3(k)+\beta x_4(k))^2+\lambda} \quad (82)$$

Now, using (81) and (82) we obtain

$$r_cx'''_3(k) - r_vx'''_4(k) = -\gamma x_3(k) - \delta x_4(k) - \nu\sqrt{(\alpha x_3(k)+\beta x_4(k))^2+\lambda} \quad (83)$$

where

$$\gamma = -(r_c(-r_cG_c+1)^2 - 2r_c^2r_vG_cG_v + r_cG_v^2r_v^2 + \alpha(1+r_vG_v-r_cG_c)) \quad (84)$$

$$\delta = -(-r_vr_c^2G_c^2 + 2r_v^2r_cG_vG_c - r_v(-r_vG_v+1)^2 + \beta(1+r_vG_v-r_cG_c)) \quad (85)$$

$$\nu = -(1+r_vG_v-r_cG_c) \quad (86)$$

Next, using $x'''_2(k) = x_2(k) + x'_4(k)\Delta t_1$, (60) and (76), it follows that

$$x'''_2(k) = x_2(k) + \frac{1}{r_c\tau/I_c}(r_cG_vx_3(k) - r_vG_vx_4(k) + x_4(k)) \times\left(\alpha x_3(k)+\beta x_4(k)+\sqrt{(\alpha x_3(k)+\beta x_4(k))^2+\lambda}\right) \quad (87)$$

Thus, equation (80) can be rewritten as

$$\Delta t_2(x_2(k),x_3(k),x_4(k)) = \frac{\gamma x_3(k)+\delta x_4(k)+\nu\sqrt{(\alpha x_3(k)+\beta x_4(k))^2+\lambda}}{r_c\tau/I_c} + \frac{1}{(r_c\tau/I_c)}\left(\gamma x_3(k)+\delta x_4(k)+\nu\sqrt{(\alpha x_3(k)+\beta x_4(k))^2+\lambda}\right)^2 + 4r_v(r_cG_vx_3(k) - r_vG_vx_4(k) + x_4(k)) \times\left(\alpha x_3(k)+\beta x_4(k)+\sqrt{(\alpha x_3(k)+\beta x_4(k))^2+\lambda}) + \mu\right)^{1/2} \quad (88)$$

where $\mu \triangleq \mu(x_2(k)) = (r_c\tau/I_c)(r_c\alpha_c + 4r_vx_2(k))$. Finally, it follows from (64) using (76) and (88) that

$$\begin{bmatrix}x_2(k+1)\\x_3(k+1)\\x_4(k+1)\end{bmatrix} = A\begin{bmatrix}x_2(k)\\x_3(k)\\x_4(k)\end{bmatrix} + \begin{bmatrix}(1/(r_c\tau/I_c))\tilde{g}(x_3(k),x_4(k))\bar{g}(x_2(k),x_3(k),x_4(k))\\(-G_c+(1/r_c))(\alpha x_3(k)+\beta x_4(k)+\sqrt{(\alpha x_3(k)+\beta x_4(k))^2+\lambda})\\-G_v(\alpha x_3(k)+\beta x_4(k)+\sqrt{(\alpha x_3(k)+\beta x_4(k))^2+\lambda})\end{bmatrix} + \begin{bmatrix}(1/(r_c\tau/I_c))\tilde{f}(x_2(k),x_3(k),x_4(k))\bar{f}(x_2(k),x_3(k),x_4(k))\\(1/r_c)(\gamma x_3(k)+\delta x_4(k)+\nu\sqrt{(\alpha x_3(k)+\beta x_4(k))^2+\lambda})\\0\end{bmatrix} + \begin{bmatrix}0\\(1/r_c)\hat{f}(x_2(k),x_3(k),x_4(k))\\0\end{bmatrix} \quad (89)$$

where

$$\left.\begin{aligned}\tilde{g}(x_3(k),x_4(k)) &= r_cG_vx_3(k) - r_vG_vx_4(k) + x_4(k)\\ \bar{g}(x_2(k),x_3(k),x_4(k)) &= \alpha x_3(k)+\beta x_4(k) + \sqrt{(\alpha x_3(k)+\beta x_4(k))^2+\lambda}\\ \tilde{f}(x_2(k),x_3(k),x_4(k)) &= \xi x_3(k)+\zeta x_4(k) - G_v\sqrt{(\alpha x_3(k)+\beta x_4(k))^2+\lambda}\\ \bar{f}(x_2(k),x_3(k),x_4(k)) &= \gamma x_3(k)+\delta x_4(k) + \nu\sqrt{(\alpha x_3(k)+\beta x_4(k))^2+\lambda}\\ &\quad +\hat{f}(x_2(k),x_3(k),x_4(k))\\ \hat{f}(x_2(k),x_3(k),x_4(k)) &= ((\gamma x_3(k)+\delta x_4(k)\\ &\quad +\nu\sqrt{(\alpha x_3(k)+\beta x_4(k))^2+\lambda})^2\\ &\quad +4r_v\tilde{g}(x_3(k),x_4(k))\bar{g}(x_2(k),x_3(k),x_4(k))+\mu)^{1/2}\\ \xi &= r_c^2G_vG_c - r_cG_v - \alpha G_v + (-r_vG_v+1)r_cG_v\\ \zeta &= -r_cr_vG_cG_v - \beta G_v + (-r_vG_v+1)^2\end{aligned}\right\} \quad (90)$$

Now, using (89) we can characterize the functions $f_2(x_2(k),\ x_3(k),\ x_4(k))$, $f_3(x_2(k),\ x_3(k),\ x_4(k))$, and $f_4(x_2(k),\ x_3(k),\ x_4(k))$ appearing in (50); namely

$$f_2(x_2(k),x_3(k),x_4(k)) = \hat{a}_{11}x_2(k)+\hat{a}_{12}x_3(k)+\hat{a}_{13}x_4(k) + \frac{1}{r_c\tau/I_c}\tilde{g}(x_3(k),x_4(k))\bar{g}(x_2(k),x_3(k),x_4(k)) + \frac{1}{r_c\tau/I_c}\tilde{f}(x_2(k),x_3(k),x_4(k))\bar{f}(x_2(k),x_3(k),x_4(k)) \quad (91)$$

$$f_3(x_2(k),x_3(k),x_4(k)) = \hat{a}_{21}x_2(k)+\hat{a}_{22}x_3(k)+\hat{a}_{23}x_4(k) + \omega\sqrt{(\alpha x_3(k)+\beta x_4(k))^2+\lambda} + \frac{1}{r_c}\hat{f}(x_2(k),x_3(k),x_4(k)) \quad (92)$$

$$f_4(x_2(k),x_3(k),x_4(k)) = \hat{a}_{31}x_2(k)+\hat{a}_{32}x_3(k)+\hat{a}_{33}x_4(k) - G_v\sqrt{(\alpha x_3(k)+\beta x_4(k))^2+\lambda} \quad (93)$$

where $\omega = (\nu/r_c) - G_c + (1/r_c)$ and $\hat{a}_{ij}$ denotes the (i, j) component of the matrix $\hat{A}$ given by

$$\hat{A} = A + \begin{bmatrix} 0 & 0 & 0 \\ 0 & \alpha(-G_c + (1/r_c)) & \beta(-G_c + (1/r_c)) \\ 0 & -\alpha G_v & -\beta G_v \end{bmatrix} + \begin{bmatrix} 0 & 0 & 0 \\ 0 & \gamma/r_c & \delta/r_c \\ 0 & 0 & 0 \end{bmatrix} \quad (94)$$

References

Andronov, A. A., Vitt, A. A., and Khaikin, S. E., 1966, *Theory of Oscillators* (New York: Dover Publications).

Bainov, D. D., and Simeonov, P. S., 1989, *Systems with Impulse Effect: Stability, Theory and Applications* (England: Ellis Horwood Limited).

Bernstein, D. S., 2002, Feedback control: An invisible thread in the history of technology. *Control Systems Magazine*, **22**, 53–68.

Brogliato, B., 1999, *Nonsmooth Mechanics* (Berlin: Springer-Verlag).

Bupp, R. T., Bernstein, D. S., Chellaboina, V., and Haddad, W. M., 2000 a, Resetting virtual absorbers for vibration control. *Journal of Vibration Control*, **6**, 61–83.

Bupp, R. T., Bernstein, D. S., Chellaboina, V.-S., and Haddad, W. M., 2000 b, Finite-time stabilization of the double integrator using a virtual trap-door absorber. *IEEE Transactions on Automatic Control*, **45**, 776–780.

Chellaboina, V., Bhat, S. P., and Haddad, W. M., 2003, An invariance principle for nonlinear hybrid and impulsive dynamical systems. *Nonlinear Analysis: Theory Methods Applications*, **53**, 527–550.

Gazely, W. J., 1956, *Clock and Watch Escapements* (London: Heywood).

Gimpel, J., 1976, *The Medieval Machine: The Industrial Revolution of the Middle Ages* (New York: Penguin Books).

Grizzle, J. W., Abba, G., and Plestan, F., 2001, Asymptotically stable walking for biped robots: Analysis via systems with impulse effects. *IEEE Transaction on Automatic Control*, **46**, 51–64.

Haddad, W. M., Chellaboina, V., and Kablar, N. A., 2001a, Nonlinear impulsive dynamical systems Part I: Stability and dissipativity. *International Journal of Control*, **74**, 1631–1658.

Haddad, W. M., Chellaboina, V., and Kablar, N. A., 2001 b, Nonlinear impulsive dynamical systems Part II: Stability of feedback interconnections and optimality. *International Journal of Control*, **74**, 1659–1677.

Headrick, M. V., 2002, Origin and evolution of the anchor clock escapement. *Control Systems Magazine*, **22**, 41–52.

Isidori, A., 1995, *Nonlinear Control Systems* (Berlin: Springer-Verlag).

Khalil, H. K., 1996, *Nonlinear Systems* (Upper Saddle River, NJ: Prentice Hall).

Lakshmikantham, V., Bainov, D. D., and Simeonov, P. S., 1989, *Theory of Impulsive Differential Equations* (Singapore: World Scientific).

Landes, D. S., 2000, *Revolution in Time: Clocks and the Making of the Modern World* (Cambridge: revised and enlarged edition, Harvard University Press).

Lepschy, A. M., Mian, G. A., and Viaro, U., 1992, Feedback control in ancient water and mechanical clocks. *IEEE Transactions on Education*, **35**, 3–10.

Mayr, O., 1970, *The Origins of Feedback Control* (Cambridge: MIT Press).

Nersesov, S. G., Chellaboina, V., and Haddad, W. M., 2002, A generalization of Poincaré's theorem to hybrid and impulsive dynamical systems. *International Journal of Hybrid Systems*, **2**, 35–51.

Penman, L., 1998, *Practical Clock Escapements* (Shingle Springs: Clockworks Press Int.).

Sobel, D., and Andrewes, W. J. H., 1998, *The Illustrated Longitude* (New York: Walker and Co.).

Ye, H., Michel, A. N., and Hou, L., 1998. Stability analysis of systems with impulsive effects. *IEEE Transactions on Automatic Control*, **43**, 1719–1723.